Functional Materials 11, No.3 (2004) © 2004 — Institute for Single Crystals

Influence of Si on microstructure and mechanical properties of TiAlSiN hard thin films

O.I.Nakonechna, M.I.Zakharenko [*]

IPMC-FSB, Swiss Federal Institute of Technology Lausanne (EPFL), Switzerland
[*]T.Shevchenko Kyiv National University, Physics Department, 6 Acad. Glushkov Ave., 03022 Kyiv, Ukraine

Structural and mechanical properties of nanocomposite TiAl(Si)N thin films prepared using arc-plasma PVD deposition technique on WC–Co substrates have been characterized by X-ray diffraction and nanoindentation. TEM have been used to study the microstructure of thin films, in order to understand the growth mechanism thereof. The maximum hardness of thin films was observed for materials of near the Al–Si eutectic composition. The smallest grain size (30 nm) in the film corresponds also to that composition.

Методами рентгеновского фазового анализа и наноиндентирования исследованы структурные и механические свойства нанокомпозитных тонких пленок на основе TiAlSiN. Материалы получены методом катодного осаждения на подложку WC–Co. Для выяснения механизма роста тонких пленок проведены электронно-микроскопические исследования. Обнаружено, что максимальная твердость тонких пленок наблюдается для материалов с химическим составом вблизи области эвтектики Al–Si. Также этому составу соответствует наименьший размер кристаллита в пленке (30 нм).

Multicomponent coatings based on different metallic and non-metallic elements combine the benefits of individual components resulting in a further improvement of the coating properties. Titanium aluminum nitride was developed in the late 1980's as a promising alternative to TiN coatings for cutting and forming tools [1]. Metastable TiAlN materials exhibit not only superior high-temperature oxidation resistance compared to TiN and better cutting behavior enabling the use of higher cutting speeds [2] but also very interesting physical properties. Several papers reported that the properties of those coatings depend on the Ti:Al ratio [3, 4]. Accordingly, the hardness increases monotonously with increasing Ti content up to approximately 60 at. % of the total metal content while it decreases sharply again at Ti content above 70 at. %. The hardness decrease at higher Ti content is connected to the decreasing effect of solution hardening of the face-centred cubic TiN-like structure of the $Ti_{1-x}Al_xN$ solid solution. At a Ti content lower than 20 at. %, the hexagonal wuertzite structure of AlN is formed [5]. Addition of Si to TiAlN coatings results in improved mechanical properties and pronounced structural refinement [6]. Structural refinement (the formation of nanograins) in TiAlN films was reported by Shieh [7]. The grain size in the films decreased to less than 10 nm as the aluminum content in the film increased up to the Al/(Al + Ti) ratio of 0.63. In HRTEM micrographs, the authors [7] observed crystalline nanograins separated by disordered grain boundaries resulting from high concentration of Al in the coating, however no amorphous matrix could be detected. Christiansen et al. [8] succeeded in producing nanocomposites made of crystalline TiN grains embedded in an amorphous SiN_x matrix. They determined the dependence of the

nanograins size on Si content in the film. For Si content close to 6 at. %, the grain size decreased to about 5 nm.

The purpose of the present study is to investigate the addition of silicon to the TiAlN coatings and its influence on the microstructure and mechanical properties. To that end, X-ray diffraction (XRD), conventional transmission electron microscopy (TEM) and high resolution one (HRTEM) and nanoindentation experiments have been carried out.

Studies specimens were TiAlSiN thin films of about 2 μm thickness deposited onto WC–Co substrates using cathodic arc physical vapour deposition (PVD) method [9]. The thin film chemical composition was analysed by Rutherford backscattering spectroscopy (RBS) and particle induced X-ray emission (PIXE) using a 2 MeV proton beam and a 2 MeV He^+ one, respectively. A Rigaku X-ray diffractometer (Cu K_α radiation, 35 kV, 40 mA at 4° grazing incidence) was employed to determine the phases and crystalline structures of the thin films. The samples were fixed at a grazing angle of 4° with respect to the incident X-ray beam and the detector was scanned along the 2θ cycle in the plane of diffractometer to record the Bragg-diffracted X-rays. The step width was 0.02° in the range of 30–100° and the acquisition time per step was 10 s.

To prepare TEM foils for transverse observations, the coated samples were first cut by a diamond wire saw to obtain slices of 500 to 800 μm thickness. These slices were thinned by mechanical polishing on diamond pads up to about 40 μm and then subjected to ion-milling for final thinning up to transparency to the electron beam. The crystalline structure of the films was analysed by TEM and HRTEM (Philips CM300), bright and dark field imaging as well as selected area electron diffraction (SAED). The hardness (H) and elastic modulus (E) of the film/substrate system were measured using a Nanoindenter XP system with a Berkovich indenter tip. The instrument was operated in continuous stiffness measurements (CSM) to measure the dependence of H and E on the indentation depth. In all CSM depth-sensing experiments, 9 tests were averaged to define mean H and E values. The analysis of nano-indentaion data followed the approach of Oliver and Pharr [10].

Table summarizes the overall chemical composition of the investigated thin films. The following remarks concerning the analysis can be made:

1. It is very difficult to determine the ratio between Al and Si using RBS. The concentration of the total amount of Al and Si is more accurate than the individual values.

2. The uncertainty in the Ti concentration is about 1 at. %; in the Al + Si concentration, about 2 at.%; and that in the N concentration, about 3 at.%. Samples Nos.1 to 4 were produced as SL materials without Si (No.1) and with Si addition (Nos.2 to 4) in order to observe possible changes in the microstructure and the mechanical properties of the coatings.

Fig. 1 shows some selected XRD patterns. The broad diffracted peaks are characteristic for nanocrystalline structure. For the Al-rich SL TiAlN sample (No.1), the typical phases are *fcc* AlN and a small amount of *fcc* TiN. Increasing the Ti content (samples Nos.5 and 6) results in formation of *fcc* Ti_3AlN accompanied by simultaneous disappearance of the AlN phase. The integral intensity of Ti_3AlN peaks increases and their widths decrease with increasing Ti-content, which corresponds to increasing crystalline volume fraction and decreasing average crystallite size. The formed phases are in accordance with Hagg rules [11]. The average crystallite sizes were determined from line broadening using the classical William-

Table. Samples' identification, chemical composition and mechanical properties of investigated thin films

Sample No.	Ti, at. %	Al, at. %	Si, at. %	N, at. %.	Al + Si, at. %	Si:Al	H, GPa	E, GPa
1	19	31		50	32		29.4	464.2
2	22	28	2	48	30	0.071	30.6	368.4
3	18	27	4	51	35	0.148	32.5	376.2
4	19	26	5	50	31	0.192	32.1	392.4
5	34	15		50	15		36.2	520.4
6	28	20	4	48	24	0.200	38.6	510.0

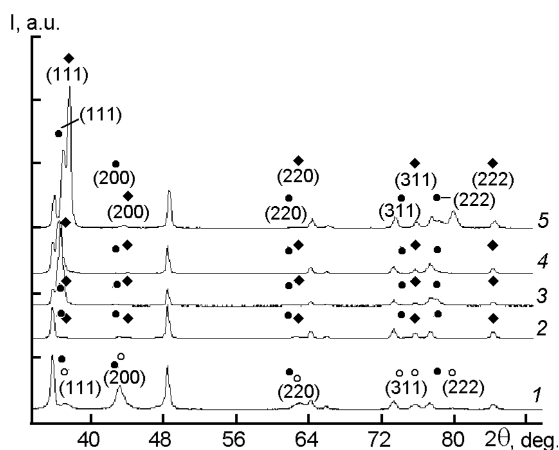

Fig. 1. XRD patterns corresponding to SL (No. 1, 2, 3), NC (No. 4) and ML (No. 5) thin films. The symbols ♦, ● and o denote the Bragg peaks of the Ti_3AlN, TiN, and AlN phases, respectively. Unindexed peaks belong to the substrate.

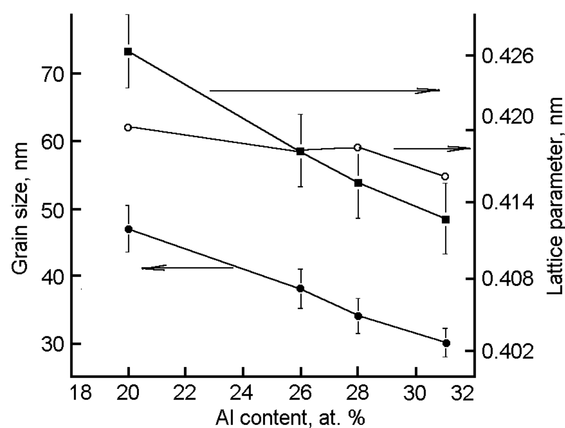

Fig. 2. Average crystallite size and lattice parameter for *fcc* AlN phase as a function of the Al-content for Al-rich SL thin films. The symbol o denotes the lattice parameter estimated from the Vegard's law.

son-Hall plot [12]. Fig. 2 shows that the average crystallite size of the *fcc* AlN phase for the coatings decreases with increasing Al content. The lattice parameter was also determined for the AlN phase using the exact Bragg positions of four strongest peaks. The lattice parameters determined from peak positions follow the predicted values of *fcc* AlN, but with some deviation (see Fig. 2).

To understand the deviation from the pure *fcc* AlN value (a = 0.40832 nm [13]), the atomic sizes should be considered. The 12-coordinated metallic (Goldschmidt) radii R_{G12} [14] of the sample constituents are as follows: R_{G12}(Al) = 0.1432 nm and R_{G12}(Ti) = 0.1462 nm. According to the equilibrium phase diagram of the Al–Ti system [15], the solubility of Ti in Al is restricted (about 1 at.% Ti), however, in nanostructured alloys and compounds, it may increase drastically up to several tens of atomic per cent [16].

Therefore, basing on the above data, it can be expected that the lattice constant of *fcc* AlN increases if Ti atoms are dissolved substitutionally. Assuming the Vegard law (VL) [14] is valid and using a (*fcc* TiN) = 0.4318 nm [13], the lattice constant of the Al-rich thin films would be a_{VL} = 0.41865 nm, 0.41630 nm, 0.41823 nm and 0.42029 nm for samples Nos. 2, 3, 4, and 6, respectively. Although the experimental lattice constants of the Al-rich coatings are somewhat smaller than those obtained from Vegard law (Δa = 0.003 to 0.035 nm), for most cases, the deviation is within the experimental error.

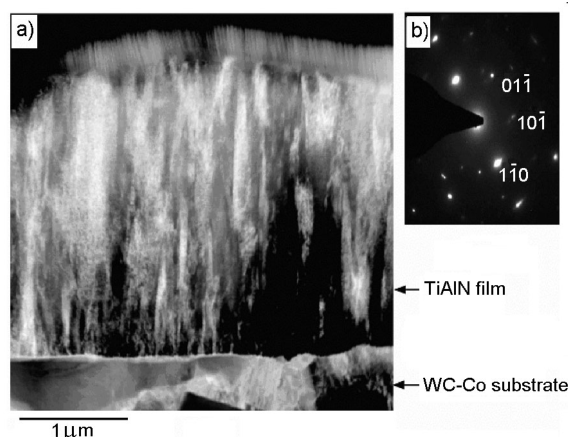

Fig. 3. STEM dark field photograph of the microstructure of the Al-rich SL (3) coating. A pronounced, uniform columnar growth can be observed. The corresponding SAED pattern belongs to [111] zone.

The micrographic view of a single layer Al-rich SL (No.1) coating is shown in the scanning transmission electron microscopy (STEM) dark field photograph, Fig. 3,a. The film is characterized by a weak columnar growth. The selected area electron diffraction (SAED) pattern of the zone [111] seen in Fig. 3,b exhibits only spots due to the large size of columns. This confirms the presence of spots belonging to the *fcc* AlN phase detected also by X-ray diffraction (see Fig. 1).

Fig. 4,a shows some selected examples of load-displacement data, which can serve to

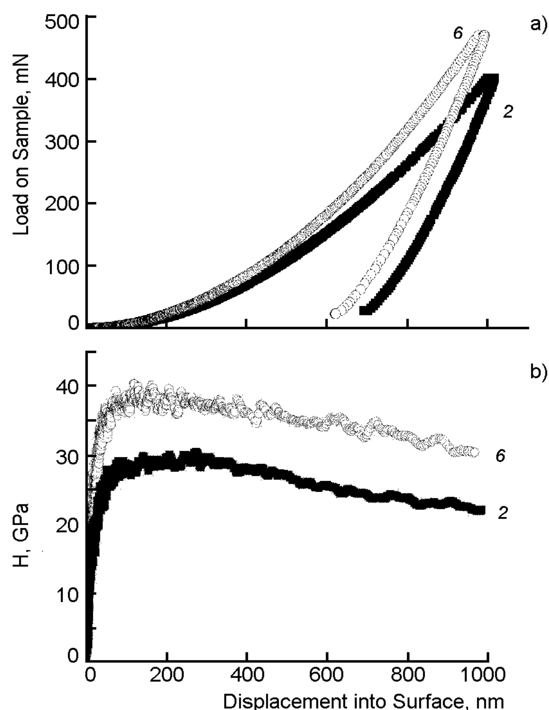

Fig. 4. Indentation load-displacement (a) and calculated hardness-displacement curves (b) corresponding to Ti-rich SL No.6 and to Al-rich SL No.2 samples. Film thickness 2 μm.

define experimental quantities based on the most widely used Oliver and Pharr analysis [10]. The loading-unloading curves exhibit similar features, the maximum indentation depth was chosen 1000 nm for each measurement. However, there is a slight difference in maximum indentation load (456 mN and 404 mN for samples Nos.6 and 2, respectively), indicating that the Al-rich film is the softest one while the Ti-rich one, the hardest.

The hardness vs. indentation depth curves evaluated from the load-displacement data are plotted in Fig. 4,b. It is seen that the hardness remains roughly constant at shallow indentations ($h < 200$ nm), and then decreases gradually. The decrease in hardness at larger indentation depth can be explained by several factors, such as influence of the substrate, indentation size effect associated with plastic deformation around the indenter as well as formation of microcracks within the film [17].

The hardness and modulus values determined from measured hardness-displacement nanoindentation curves (see Fig. 4,b) are listed in Table and plotted in Fig. 5 as a function of the relative Si:Al content. The

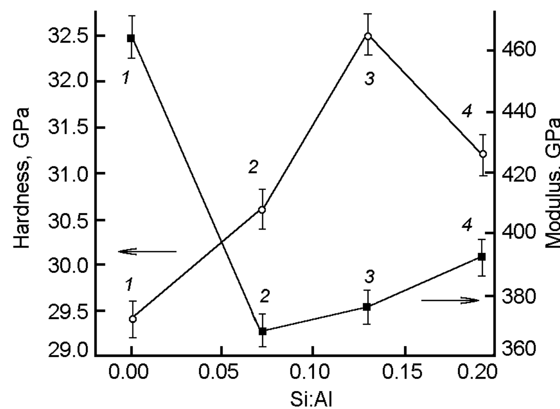

Fig. 5. Dependence of the measured hardness (H) and Young modulus (E) on the relative Si:Al atomic content for SL Al-rich thin films (Nos 1–4).

hardness exceeds 29 GPa for all investigated samples. As it is seen, Si addition to the Al-rich TiAlN single-layer coatings (samples Nos.1 to 4) results in the increase of hardness and Young modulus values. The H values exhibit a maximum at relative Si:Al atomic concentration 0.13 which value is close to the Si–Al eutectic concentration [15] and corresponds to the smallest AlN average grain size (30 nm).

The observed hardness maximum can be correlated with bonding characteristics of the constituent elements [11]. The bulk modulus increases as the nearest neighbor distance in AB compound decreases. Assuming that the increase of bulk modulus corresponds to the increase in hardness, the increase in hardness of the compound can be explained by a decrease in interatomic distances due to addition of Al. The interatomic distance (d) is related to the covalent band gap (E_h) according to the expression $E_h = Kd^{-2.5}$. Therefore, the origin of hardness increase is probably related to an increase of covalent energy in investigated films. As it is seen in Table, the sample No.3 is the richest in Al, and therefore exhibits the shortest interatomic distances.

Ti-rich TiAlN coating (No.5) possesses remarkably higher hardness and modulus values as compared to Al-rich film (No.1) which can correspond to the formation of the *fcc* TiN and Ti_3AlN phases which exhibit higher hardness. The subsequent addition of Si (No.6) further improves the mechanical properties.

Thus, the, microstructure characterization of single layer, multilayer, and gradient nanocomposite TiAl(Si)N thin films

has shown that Al-rich coatings contain AlN and TiN phases. The Al content influences only slightly the lattice parameter of the (Al,Ti)N phase and results in Ti_3AlN phase formation and the disappearance of AlN phase. The average crystallite size increases with increasing Ti content. TEM investigations have shown that Al-rich single layer films are characterized by a weak columnar structure. Si addition into TiAlN films results in generation of nanocomposite structures by forming nanograins embedded into a matrix. The role of Si in structural refinement has been analyzed. nanoindentation measurements revealed that the hardness of Al-rich single layers shows a maximum at about the eutectic Al–Si composition that can be explained in terms of bonding characteristics.

References

1. W.D.Munz, *J. Vac. Sci. Technol.*, **A4**, 2717 (1986).
2. O.Knotek, M.Bohmer, T.Leyendecker, *J. Vac. Sci. Technol.*, **A4**, 2695 (1986).
3. Y.Tanaka, T.M.Gur, M.Kelly, *J. Vac. Sci. Technol.*, **A10**, 1749 (1992).
4. A.Kimura, H.Hasegawa, K.Yamada, T.Suzuki, *Surf. Coat. Technol.*, **120/121** 438 (1999).
5. E.Vancoille, J.P.Celis, J.R.Roos, *Thin Solid Films*, **224**, 168 (1993).
6. S.Veprek, *Thin Solid Films*, **317**, 449 (1998).
7. A.Shieh, M.H.Hon, *Thin Solid Films*, **391**, 101 (2001).
8. S.Christiansen, M.Albrecht, H.P.Strunk, *Am. Vac. Soc.*, **B16(1)**, 19 (1998).
9. A.Karimi, Y.Wang, T.Cselle, M.Morstein, *Thin Solid Films*, **420/421**, 275 (2002).
10. W.C.Oliver, G.M.Pharr, *J. Mater. Res.*, **7**, 1564 (1992).
11. L.E.Toth, Transition Metal Carbides and Nitrides, Academic Press Inc., New York, London (1971).
12. H.P.Klug, L.E.Alexander, X-ray Diffraction Procedures for Polycrystalline and Amorphous Materials, Wiley, New York (1974).
13. P.Villars, L.D.Calvert, Pearson's Handbook of Crystallographic Data for Intermetallic Phases, American Society of Metals, Metals Park, Ohio (1985).
14. W.B.Pearson, The Crystal Chemistry and Physics of Metals and Alloys, Wiley-Interscience, New York (1972).
15. T.B. Massalski (Ed.), Binary Alloy Phase Diagrams, 2nd Ed., plus updates on CD-ROM, ASM International, Materials Park, Ohio (1996).
16. K.Hono, Y.Zhang, P.Tsai et al., *Scripta Met. Mat.*, **32**, 191 (1995).
17. O.R.Shojaei, A.Karimi, *Thin Solid Films*, **332**, 202 (1998).

Вплив Si на мікроструктуру та механічні властивості тонких плівок на основі TiAlSiN

О.І.Наконечна, М.І.Захаренко

Методами рентгенівського фазового аналізу та наноіндентування досліджено структуру та механічні властивості нанокомпозитних тонких плівок на основі TiAlSiN. Матеріали одержано методом катодного осадження на підкладку WC–Co. З метою визначення механізму росту тонких плівок проведено електронно-мікроскопічні дослідження. Максимальна твердість плівок спостерігається для зразків, хімічний склад яких знаходиться поблизу області евтектики Al–Si. Цьому складу відповідає також і мінімальний розмір кристалітів (30 нм).